Nonlinear Dynamics and Systems Theory, **11** (4) (2011) 425–438

Improved Multimachine Multiphase Electric Vehicle Drive System Based on New SVPWM Strategy and Sliding Mode — Direct Torque Control

N. Henini [1*], L. Nezli [1], A. Tlemçani [2] and M.O. Mahmoudi [1]

[1] *Laboratory of Processes Control, National Polytechnic School, 10, Ave, Hassen Badi, BP 182, El-Harrach, Algiers, Algeria*
[2] *Laboratory of Research in Electrotechnic and Automatic, Ain D'heb, Medea, Algiers, Algeria*

Received: January 14, 2011; Revised: September 28, 2011

Abstract: This paper presents a Sliding Mode Direct Torque Control (SM-DTC) of a multiphase Induction Machine (IM) supplied with multiphase voltage source inverter (VSI) controlled by a new algorithm of Space Vector Pulse Width Modulation (SVPWM) for a high-performance multi-machine electric vehicle (EV) drive system. The SM-DTC is one of the effective nonlinear robust control approaches; it provides better dynamic performances of considered system. The new SVPWM algorithm develops a new analysis of voltage vectors to synthesize required phase voltages for driving multiphase IM with a minimum switch stress. Theoretical developments are verified for EV with two-separate-wheel-drives based on two pentaphase induction motors. The obtained results illustrate the effectiveness of the proposed drive system. Moreover, this system can be easily extended to an n-phase multi-machine drive system.

Keywords: *multiphase multimachine drive system; multiphase SVPWM; multiphase VSI; sliding mode; direct torque control.*

Mathematics Subject Classification (2000): 93C10, 93C85.

* Corresponding author: mailto:henini_nour@yahoo.fr

1 Nomenclatures

s, r	: Stator, rotor indexes.
α, β	: Fixed stator reference frame indexes.
ref	: Reference index.
V, i, Φ	: Voltage, current, flux.
L	: Inductance.
R	: Resistance.
M	: Mutual inductance.
σ	: Total leakage coefficient.
n_p	: Pole pair number.
v	: Vehicle speed.
r	: Wheel radius.
$2d$	: Traction axle Length.
ρ	: Radius of way curvature.
ω	: Vehicle rotation speed.
Ω	: Motor speed.
Ω_R, Ω_L	: Speed of right and left motors.
Ω_R^*, Ω_L^*	: Reference speed of right and left motors.
T_{eR}^*, T_{eL}^*	: Reference torque of right and left motors.
T_i	: Simple time.
T_L	: Load torque.
y_1, y_2	: estimated stator flux components

2 Introduction

The research on development of electrical road vehicles aims to solve environment and energy problems caused by using the internal combustion engine vehicles (ICV). The first ones present many advantages as compared with the ICV ([1]– [8]).

The principal advantage of EV is the electric motor drive system. Thus, the trend within EV technology today is to develop Alternative Current (AC) motor drive systems for the next generation of such vehicles due to reduced size, weight, volume and maintenance.

The induction motors (IM) are relatively of a high reliability, high efficiency even in high speed range and low production cost. Therefore much attention is given to their control for various applications with different control requirements [2].

Recently, The Direct Torque Control (DTC) is more frequent in IM control. It is based on the decoupled control of stator flux and torque providing a quick and robust response with a simple control construction in AC drive ([5]– [9]). However, the conventional DTC presents a serious problem in low speed and in variation of motor parameters sensivity [10].

This paper presents a traction drive system for EV with two-independent-wheel-drives. This system includes two pentaphase induction motor drives controlled using hybrid control (SM-DTC). This control is one of the most effective nonlinear robust control approaches; it provides good dynamic performances of considered system [15]. In addition, this paper presents a new analysis of multiphase SVPWM for whatever number of phases. In order to synthesize an arbitrary phase voltage in terms of the times applied to the available switching vectors, the concept of orthogonal multi-dimensional vector space is used. An appropriate vector sequences are chosen to minimize switching losses.

Throughout this paper, the proposed algorithm is applied for supplying the pentaphase multimachine system proposed. The basic concepts can be easily extended to an n-phase system. The computational cost of the proposed strategy is low; it is well suited for real-time hardware implementation. The obtained results illustrate that with this configuration of EV Drive, it is possible to improve the stability of the vehicle under road conditions without any complicated mechanical components. Replacing the usual mechanical differential by an Electrical Differential (ED) is the solution to face the disadvantage of mechanical differential. This possibility is taken into consideration in this paper; the solution of ED is tested under different ways: straight-line, left and right turning.

3 Vehicle with Two-Separate-Wheel-Drives

The proposed EV Drive control can be used for all electric traction systems with two separate wheels drives. This system includes the elements represented in Figure 1. In this structure we find: two induction motors, two PWM inverters, the mechanic transmission system (motor to wheel), batteries, and control unit [3]. It is clearly noted that this topology of structure reduces the mechanic transmission components (mechanical differential operation is assured by an adequate control strategy of the two motors). Besides, this configuration offers the following advantages:

- Relatively, a good maneuverability: the torques of the two motors can be controlled independently precisingly and quickly.
- Elimination of mechanical differential.
- A good repartition of drive power.
- With other castor wheels used, the drive wheels can be the directional wheels.

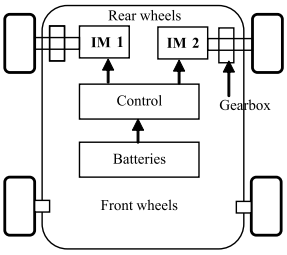

Figure 1: Traction system for electric vehicle with two-independent-wheel-drives.

4 Traction Drive System Proposed

Figure 2 illustrates the general scheme of the traction system proposed. The control of induction motors 1 and 2 are assured by SM-DTC. The torque references are generated by speed control of the two wheels, using SM controller. The speed references are generated by speed and direction orders. The speed and the direction orders are obtained, respectively, by the accelerator or brake pedals, and the steering wheel.

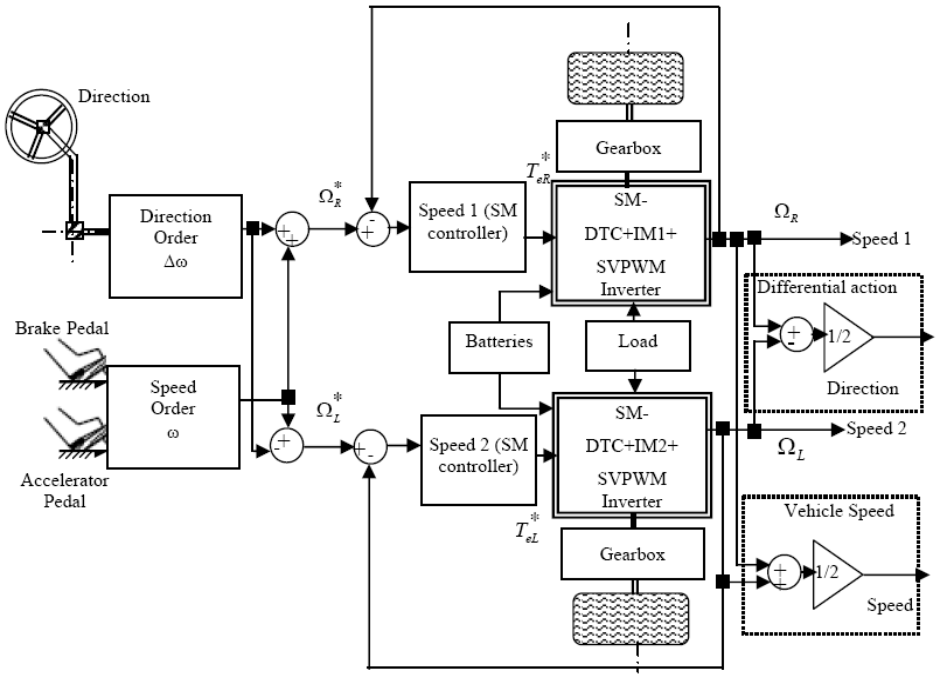

Figure 2: Scheme of the proposed drive system.

4.1 Electric differential

Figure 2 assumes that the linear speed of the vehicle v is imposed. The rotation speed for each motor depends on the type of driving regime selected.

For the straight road regime, the rotation speed for each motor becomes:

$$\Omega_L = \Omega_R = \frac{v}{r}. \tag{1}$$

For the turning regime, the angular speeds for each motor are different, for example in the left turning these speeds are expressed as [4]:

$$\Omega_L = \frac{2v}{\left(1+\dfrac{\rho+d}{\rho-d}\right)r} = \frac{v}{r} - \Delta\omega, \quad \Omega_R = \frac{2v}{\left(1+\dfrac{\rho+d}{\rho-d}\right)r} = \frac{v}{r} + \Delta\omega, \quad \Delta\omega = d.\frac{v}{\rho.r}, \tag{2}$$

where $\triangle\omega$ is imposed when the vehicle crosses a turning way.

4.2 Sliding mode – direct torque control

The Classic DTC presents the advantage of a very simple control scheme of stator flux and torque by two hysteresis controllers, which give the input voltage of the motor by selecting the appropriate voltage vectors of the inverter through a look-up-table in order to keep stator flux and torque within the limits of two hysteresis bands [5]. Figure 3 illustrates the general scheme for the classic DTC.

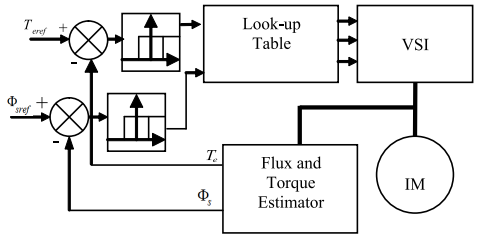

Figure 3: Basic of the Direct Torque Control Scheme.

The fast dynamic response of the classic DTC was entirely preserved, while the steady-state response was significantly improved even at a low switching frequency, but it was very sensitive to parameter uncertainties due to depending upon motor parameters.

The sliding mode control (SMC) is a very effective approach to solve the problem thanks to its well established design criteria, easy implementation, fast dynamic response, and robustness to parameter variations. Figure 4 illustrates the general scheme for the SM- DTC [11–14].

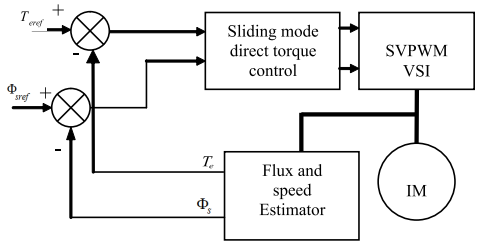

Figure 4: Structure of sliding mode DTC without switching table.

4.2.1 The induction motor model

The only difference between the five-phase motor model and the corresponding three-phase motor model is the presence of x-y component equations. Rotor x-y components are fully decoupled from d-q components and one from the other. Since rotor winding is short-circuited, x-y components cannot appear in the rotor winding. Zero sequence component equations for both stator and rotor can be omitted from further consideration due to short-circuited rotor winding and star connection of the stator winding. Finally, since stator x-y components are fully decoupled from d-q components and one from the other, the equations for x-y components can be omitted from further consideration as well. This means that the model of the five-phase induction motor in an arbitrary reference frame becomes identical to the model of a three-phase induction motor.

The induction motor model, developed in the reference frame (α, β) is described by (3). This model contains: four electrical variables (currents and flux), one mechanical

variable and two control variables (stator voltages):

$$\begin{cases} \dot{x_1} = \gamma.x_1 + \dfrac{\Gamma}{T_r}.x_3 + n_p.\Gamma.x_4.x_5 + \delta.V_{s\alpha}, \\ \dot{x_2} = \gamma.x_2 + \dfrac{\Gamma}{T_r}.x_4 - n_p.\Gamma.x_3.x_5 + \delta.V_{s\beta}, \\ \dot{x_3} = \dfrac{M}{T_r}.x_1 - \dfrac{1}{T_r}.x_3 - n_p.x_4.x_5, \\ \dot{x_4} = \dfrac{M}{T_r}.x_2 - \dfrac{1}{T_r}.x_4 + n_p.x_3.x_5, \\ \dot{x_5} = \eta.(x_2.x_3 - x_1.x_4) - \dfrac{T_L}{J}, \end{cases} \tag{3}$$

where the stator voltages and the states variables are:

$$V_s^T = [V_{s\alpha}, V_{s\beta}]^T, \qquad X^T = [x_1, x_2, x_3, x_4, x_5]^T = [i_{s\alpha}, i_{s\beta}, \Phi_{r\alpha}, \Phi_{r\beta}, \Omega]^T, \tag{4}$$

$$\begin{cases} \delta = \dfrac{1}{\sigma L_s}, \eta = \dfrac{n_p M}{J L_r}, \gamma = -\left(\dfrac{1}{\sigma T_s} + \dfrac{1-\sigma}{\sigma T_r}\right), \Gamma = \dfrac{1-\sigma}{\sigma M}, \\ \sigma = 1 - \dfrac{M^2}{L_s L_r}, T_s = \dfrac{L_s}{R_s}, T_r = \dfrac{L_r}{R_r}. \end{cases} \tag{5}$$

4.2.2 Switching surfaces selection

It is well known that the squared norm of the stator flux plays an important role in the performance of a motor and is also closely related to the electromagnetic torque. Therefore, we choose the control of the active torque u_T and the square of the flux norm $u_\Phi = \Phi^2$, which are defined as:

$$u_T = x_2.y_1 - x_1.y_2, \quad u_\Phi = y_1^2 + y_2^2. \tag{6}$$

Let's define the errors as:

$$e_1 = u_T - u_{T_{ref}}, \quad e_2 = u_\Phi - u_{\Phi_{ref}}, \tag{7}$$

where $u_{T_{ref}}$ and $u_{\Phi_{ref}}$ are the reference values of the active torque and the square of the flux norm, respectively.

The sliding-mode control is first used to find the sliding surface $S = 0$. In the present case, we adopt the integral function of the active torque and the square of the flux norm errors to obtain:

$$S_1 = e_1 + K_1 \int e_1 dt, \quad S_2 = e_2 + K_2 \int e_2 dt, \tag{8}$$

with K_1 and K_2 are positive constants.

4.2.3 Convergence conditions

So that control variables converge exponentially to their reference values, it is necessary for the surfaces to be null.

In addition, the realization of the sliding mode control is conditioned by checking the Lyaponov condition ([16]– [20]):

$$S_i.\dot{S_i} < 0, \;\; i = 1, 2, \tag{9}$$

and the invariance condition

$$\dot{S_i} = 0, \;\; i = 1, 2. \tag{10}$$

4.2.4 Switching function synthesis

Our goal is to generate a control law using the sliding mode control theory.

The derivative of the surfaces S_1 and S_2 will be:

$$\dot{S} = F + D.V, \tag{11}$$

where

$$F = \begin{bmatrix} F_1 \\ F_2 \end{bmatrix}; D = \begin{bmatrix} \frac{L_r.y_2}{\alpha.M} + x_2 & -\frac{L_r.y_1}{\alpha.M} - x_1 \\ 2.y_1 & 2.y_2 \end{bmatrix}, \tag{12}$$

$$\begin{cases} F_1 = \left(\frac{\beta}{\alpha + K_1}\right).u_T + n_p.x_5.\left(\phi_d + \frac{L_r}{\alpha.M}.u_\Phi\right) - K_1.u_{T_{ref}} - \dot{u}_{T_{ref}}, \\ F_2 = 2.R_s.\phi_d - \dot{u}_{\Phi_{ref}} - K_2.u_{\Phi_{ref}} + K_2.u_\Phi, \end{cases} \tag{13}$$

$$\alpha = M - \frac{L_s L_r}{M}, \quad \beta = \frac{L_s R_r + L_r R_s}{M}, \quad \phi_d = x_1.y_1 + x_2.y_2 \tag{14}$$

and to check the stability condition of Lyaponov, it is necessary to have:

$$\dot{S} = \mu.Sgn\,(S)\,. \tag{15}$$

By equalizing (15) and (11), we have the general control law:

$$V = -D^{-1}.\mu.Sgn\,(S) - D^{-1}.F. \tag{16}$$

We can write it as:

$$\begin{bmatrix} V_{s\alpha} \\ V_{s\beta} \end{bmatrix} = \begin{bmatrix} V_{eq\alpha} \\ V_{eq\beta} \end{bmatrix} + \begin{bmatrix} V_{c\alpha} \\ V_{c\beta} \end{bmatrix} \tag{17}$$

with definition of the equivalent control as:

$$\begin{bmatrix} V_{eq\alpha} \\ V_{eq\beta} \end{bmatrix} = -D^{-1}.\begin{bmatrix} F_1 \\ F_2 \end{bmatrix} \tag{18}$$

and the commutation control as:

$$\begin{bmatrix} V_{c\alpha} \\ V_{c\beta} \end{bmatrix} = -D^{-1}.\begin{bmatrix} \mu_1 & 0 \\ 0 & \mu_2 \end{bmatrix}.\begin{bmatrix} Sgn\,(S_1) \\ Sgn\,(S_2) \end{bmatrix}. \tag{19}$$

Because the commutation control is included in the general control, it is necessary to choose μ_1 and μ_2 large enough: $\mu_1 > |F_1|\,, \quad \mu_2 > |F_2|\,.$

4.2.5 Chattering problem

It is well known that sliding-mode technique generates undesirable chattering; this problem can be solved by replacing the switching function with the saturation function [10]:

$$Sat\,(S_i) = \begin{cases} 1, & S_i > \lambda_i, \\ -1, & S_i < -\lambda_i, \\ \frac{S_i}{\lambda_i}, & |S_i| < \lambda_i, \end{cases} \tag{20}$$

where $\lambda_i > 0$ is a smooth factor.

5 SVPWM Algorithm Development

5.1 Principal of reference vector approximation

Similar to the SVM algorithm for three phase inverters, the reference space vector is used to select the corresponding set of nearest adjacent voltage space vectors. The adjacent vectors selected can synthesize a desired reference voltage vector using averaged approximation.

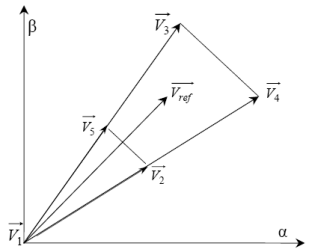

Figure 5: Generation of the reference vector by using five vectors.

If the reference vector lies in the sector connecting the tips of vectors $\overrightarrow{V_1}, \overrightarrow{V_2}, ..., \overrightarrow{V_n}$ (Figure 5), the average reference vector can be obtained with:

$$\overrightarrow{V}_{ref} = \frac{t_1}{T_i}\overrightarrow{V}_1 + \frac{t_2}{T_i}\overrightarrow{V}_2 + \frac{t_3}{T_i}\overrightarrow{V}_3 + ... + \frac{t_n}{T_i}\overrightarrow{V}_n, \tag{21}$$

where $t_1, t_2, ..., t_n$ must satisfy the condition $t_1 + t_2 + ... + t_n = T_i$.

5.2 Switching vector sets selection

From the vectors limiting one sector, we choose the sequence of vectors achieving one switch transition; there are (n+1) vectors. The sets of corresponding vectors are selected to be used in SVPWM algorithm; there are (n+1)/2 sets. For example, for seven phase inverter, Figures 6, 7, 8 present the sets selected with respect to the criteria of one switch transition, in the three plans. It is clear that the sets covered all range of reference vectors.

5.3 Applying time of switching vectors calculation

The duty cycles corresponding to voltage vectors are proportional to their distance from the reference vector.

5.4 Switching sequence arrangement

The row of applied nearest vectors depends on the sector number (even or odd). The row is showed by the arrow in Figures 9, 10 for five and seven phase inverters respectively.

For one vector approximation, the row of the elements in the sequence is reversed in the next half of the modulation period, as shown in Figures 11.

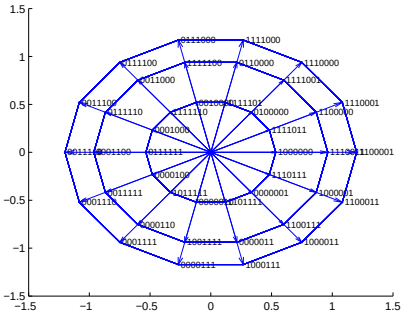

Figure 6: The sets selected for a seven phase inverter in the first plan.

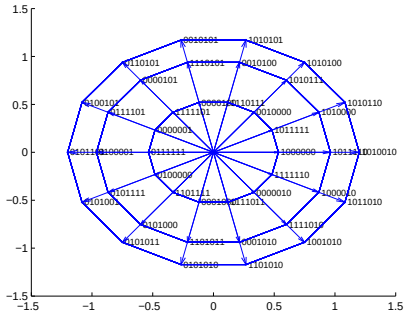

Figure 7: The sets selected for a seven phase inverter in the second plan.

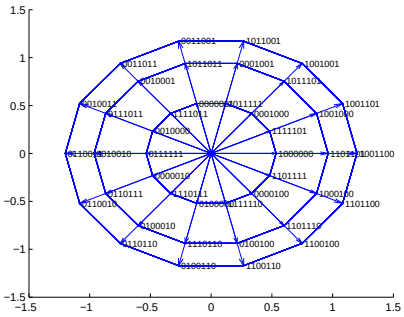

Figure 8: The sets selected for a seven phase inverter in the third plan.

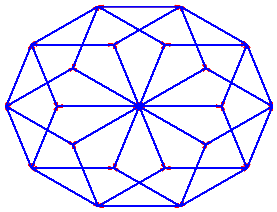

Figure 9: Vector sequence arrangement in the five phase inverter.

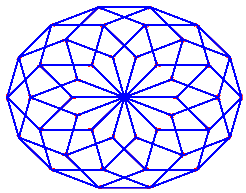

Figure 10: Vector sequence arrangement in the seven phase inverter

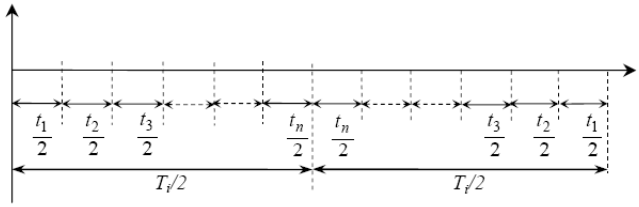

Figure 11: Switching sequence arranged in symmetrical pattern.

6 Simulation Results

6.1 Test of SVPWM strategy

To validate the proposed algorithm, simulation examples are realized for 5 and 7 phases inverters to indicate the simplicity of this algorithm for any number of phases as shown in Figures 12 to 19, which represent respectively the reference vector location (Figures 12, 16), the phase voltage (Figures 13, 17), switching sequence arrangement (Figures 14, 18), phase voltage spectrum (Figures 15, 19). Higher phases of SVM will be simulated with the same simplicity.

A deeper analysis of the resulting PWM voltage harmonics spectrum shows that the low order harmonics remain relatively weak and the increase of the phase number has an effect on the reduction of the harmonics content.

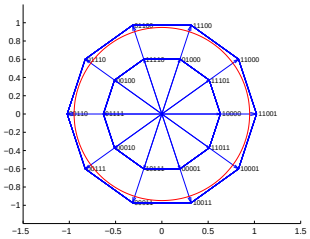

Figure 12: The reference vector location in the first plan for a five phase inverter .

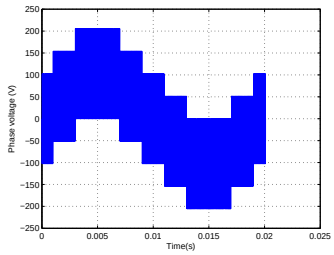

Figure 13: Phase voltage of a five-phase-VSI.

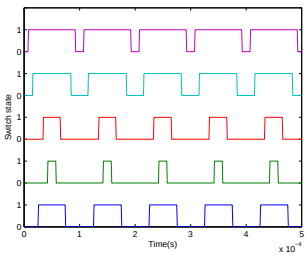

Figure 14: Switch state of a five-phase-VSI.

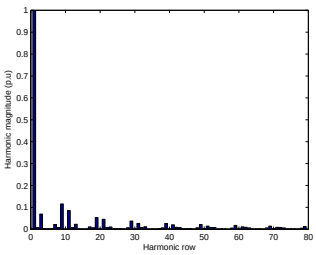

Figure 15: Phase voltage spectrum.

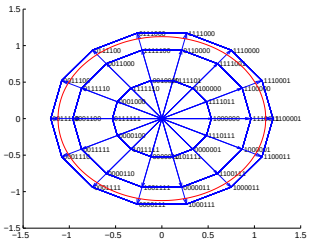

Figure 16: The reference vector location in the first plan of a seven-phase-inverter.

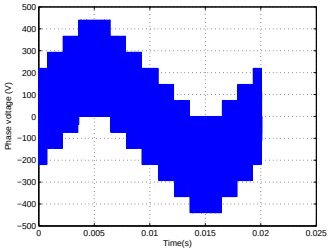

Figure 17: Phase voltage of a seven-phase-VSI.

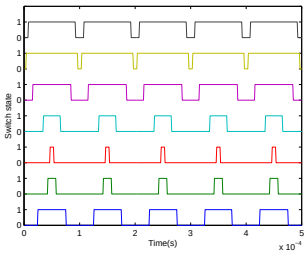

Figure 18: Switch state of a seven-phase-VSI.

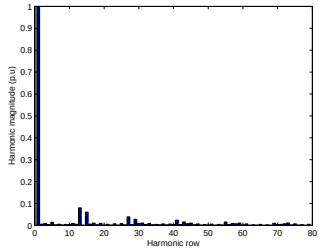

Figure 19: Phase voltage spectrum.

6.2 Test of speed and torque controls

Simulation results are obtained for a two identical squirrel cage pentaphase IM with parameters shown in the appendix. The reference speed represents the motion that the vehicle will have to cross. A trapezoidal form of speed is choosen, which allows simple calculations and also represents a realizable form. This form includes three phases:

- Phase 1: Constant acceleration; speed increases linearly.
- Phase 2: Null acceleration: constant speed.
- Phase 3: Constant acceleration; speed decreases linearly.

Figures 20, 22 and 24 represent the speed, torque and flux responses for the pentaphase induction motor respectively. The inverter phase current and the phase voltage of IM1 are shown in Figures 25, 26.

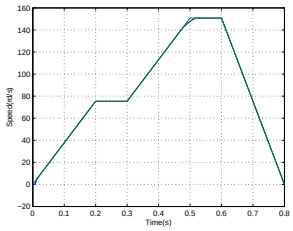

Figure 20: Motor speed.

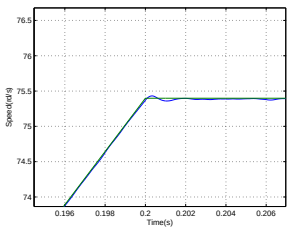

Figure 21: Motor speed zoom.

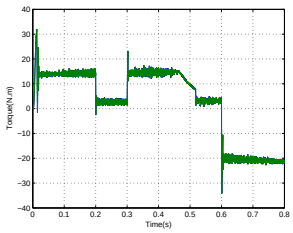

Figure 22: Motor torque.

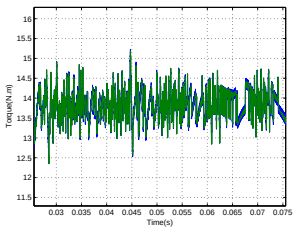

Figure 23: Motor torque zoom.

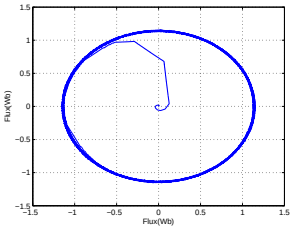

Figure 24: Motor flux.

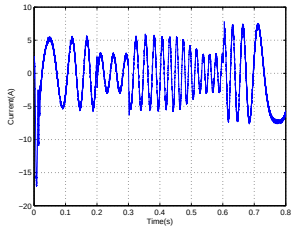

Figure 25: Stator phase current of IM1.

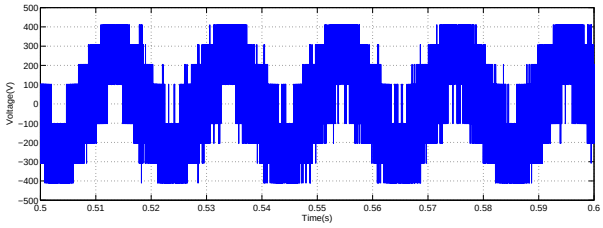

Figure 26: Inverter phase voltage.

It can be seen from Figures 20 that the motor speed tracks the reference very well and a small deviation appears only at the begining of the transient.

6.3 Test of electric differential

In order to test the performance of electrical differential used in electric vehicle, we have two interesting situations:

- The straight road regime, where both motors operate at the same speed.
- The turn regime, where each motor operates at a different speed.

Figures 27, 29 and 28, 30 represent the speed and torque responses for the two vehicle induction motors in a straight road, right and left turn. They show the follow up of the speed references and the motor speeds.

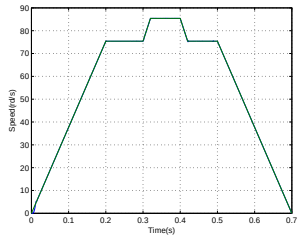

Figure 27: Right Motor speed.

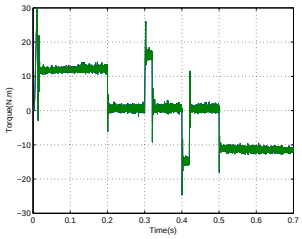

Figure 28: Right motor torque.

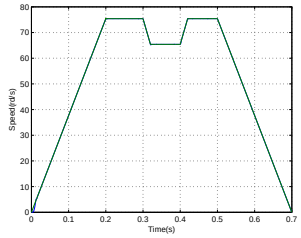

Figure 29: Left Motor speed.

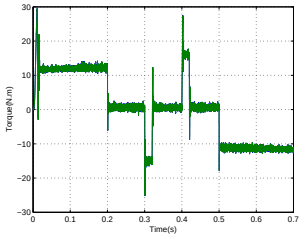

Figure 30: Left motor torque.

7 Conclusion

This paper describes a SM-DTC for a high-performance electric vehicle with two-separate-wheel-drive based on two pentaphase induction motors supplied by two pentaphase SVPWM VSIs. The proposed system aims at the elimination of hard mechanic devices (mechanic differential), and replacing it by soft ones (electric differential). Simulation tests have been carried out on a pentaphase induction motor drive. The obtained results illustrate that the sliding mode control provides a simple implementation in terms of time calculation with high performance of speed and torque response.

Appendix

Induction motors data:

Rated power	: 1Kw
Stator resistance	: 4.85 Ω
Rotor resistance	: 3.805 Ω
Stator inductance	: 0.274 H
Rotor inductance	: 0.274 H
Mutual inductance	: 0.258 H
Motor-Load inertia	: 0.031 Kg.m^2
Pole pairs	: 2

References

[1] Jahns, T. M. et al. Recent advances in power electronics technology for industrial and traction machine drives. *IEEE Proc.* **89** (6) (2001) 963–975.

[2] Zeraoulia, M. et al. Electric motor drive selection issues for HEV propulsion systems: A comparative study. *IEEE trans. Vehicular Technology* **55** (6) (2006) 1756–1764.

[3] Nobuyoshi Mutoh, Takuro Horigome, Kazuya Takita. Driving Characteristics of an Electric Vehicle System with Independently Driven Front and Rear Wheels. *EPE* (2003).

[4] Ledezma, E., Muoz-Garcia, A. and Lipo, T. A. A Dual Three-Phase Drive System with a Reduced Switch Count. *IEEE Proc.* (1998) 781–788.

[5] Takahashi and Nogushi, T. A new quick-response and high efficiency control strategy of induction motor. *Proc. IEEE Trans. Indus. Appl.* **22** (5) (1986) 820–827

[6] Khoucha, F., Marouani, K., Kheloui, A. and Aliouane, K. A DSP-based Discrete Space Vector Modulation Direct Torque Control of Sensorless Induction Machines. *IEEE Conference*, Germany, 2004.

[7] Kubota, H., Matsuse, K. and Nakmo, T. DSP-Based Speed Adaptive Flux Observer of Induction Motor. *IEEE Trans. on Ind. Appl.* **29** (2) (1993) 344–348.

[8] Chan, C. C. The state of the art of electric and hybrid vehicles. *Proc. IEEE* **29** (2) (2002) 247–275.

[9] Marouani, K. and Kheloui, A. Commande directe du couple d'une machine asynchrone par PC. *Intern. Conf. on Electrical Engineering.* Boumerdes, 2000.

[10] Bird, I. G. and H. Zelaya de la Parra. Practical evaluation of two stator flux estimator techniques for high performance direct torque control. *IET conf. Power Electronics and Variable Speed Drives* (1996) 465–470.

[11] Utkin, V. I. Sliding mode control design principles and applications to electric drives. *IEEE Trans. Ind. Electron* **40** (1) (1993) 23–36.

[12] Shiau, L. G. and Lin, J. L. Stability of sliding-mode current control for high performance induction motor position drives. *IEE Proc. Electric Power Applications* **148** (1) (2001) 69–75.

[13] Shir-Kuan, L. and Chin-Hsing, F. Sliding-Mode Direct Torque Control of an Induction Motor. *IEEE Conf. Industrial Electronics Society* (2001) 2171–2178.

[14] Benchaib, A. and Edwards, C. Nonlinaer Sliding Mode Control of an Induction Motor. *Adapt. Control Signal Process* **14** (2) (2000) 201–221.

[15] Chekireb, H., Tadjine, M. and Djemai, M. On a Class of Manifolds for Sliding Mode Control and Observation of Induction Motor. *Nonlinear Dynamics and Systems Theory* **8** (1) (2008) 21–34.

[16] Chekireb, H., Tadjine, M. and Djemai, M. Lyapunov Based on Cascaded Non-linear Control of Induction Machine. *Nonlinear Dynamics and Systems Theory* **7** (3) (2007) 253–266.

[17] Bey, W., Kardous, Z. and Braiek, N. B. On the PLF Construction for the Absolute Stability Study of Dynamical Systems with Non-Constant Gain. *Nonlinear Dynamics and Systems Theory* **10** (1) (2010) 21–28.

[18] Doan, T.S., Kalauch, A. and Siegmund,S. Exponential Stability of Linear Time-Invariant Systems on Time Scales. *Nonlinear Dynamics and Systems Theory* **9** (1) (2009) 37–50.

[19] Kovalev, A.M., Martynyuk, A.A., Boichuk, O.A., Mazko, A.G., Petryshyn, R.I., Slyusarchuk, V.Yu., Zuyev, A.L. and Slyn'ko, V.I. Novel Qualitative Methods of Nonlinear Mechanics and their Application to the Analysis of Multifrequency Oscillations, Stability, and Control Problems. *Nonlinear Dynamics and Systems Theory* **9** (2) (2009) 117–146.

[20] Leonov, G.A. and Shumafov, M.M. Stabilization of Controllable Linear Systems. *Nonlinear Dynamics and Systems Theory* **10** (3) (2010) 235–268.